Marine and Petroleum Geology 57 (2014) 509–520

Contents lists available at ScienceDirect

Marine and Petroleum Geology

journal homepage: www.elsevier.com/locate/marpetgeo

Research paper

The composition and its impact on the methane sorption of lacustrine shales from the Upper Triassic Yanchang Formation, Ordos Basin, China

Huijuan Guo [a, b], Wanglu Jia [a, *], Ping'an Peng [a], Yuhong Lei [c], Xiaorong Luo [c], Ming Cheng [c], Xiangzeng Wang [d], Lixia Zhang [d], Chengfu Jiang [d]

[a] State Key Laboratory of Organic Geochemistry, Guangzhou Institute of Geochemistry, Chinese Academy of Sciences, Guangzhou 510640, China
[b] University of Chinese Academy Sciences, Beijing 100049, China
[c] Institute of Geology and Geophysics, Chinese Academy of Sciences, Beijing 100029, China
[d] Shaanxi Yanchang Petroleum (Corporation) Company Limited, Xi'an 710075, China

ARTICLE INFO

Article history:
Received 18 April 2014
Accepted 21 May 2014
Available online 2 June 2014

Keywords:
Yanchang shales
Methane sorption
Residual bitumen
Clay minerals
Ordos Basin

ABSTRACT

The organic geochemistry, mineralogy and methane sorption of lacustrine shales of the Upper Triassic Yanchang Formation, collected from the south-eastern Ordos Basin, were investigated to characterize them and clarify the effects of shale composition on their sorbed gas capacity. These Yanchang shales have recently been selected as a target area for shale gas exploration in typical terrestrial strata in China. The two main sections of these shales containing type II organic matters, Chang 7 and Chang 9, have relatively high total organic carbon content (TOC) of 2–10%. The two shales also have similar mineralogies, mainly comprising quartz, clay minerals and feldspars. Both the Chang 7 and Chang 9 shales are generally in the oil window; Chang 9 is slightly more mature than Chang 7. Higher methane sorption capacity was observed for Chang 9 than for Chang 7 shales, determined on a dried basis at 50 °C. Methane sorption measurements were further performed on three samples from which the residual bitumen had been extracted, and their corresponding kerogen fractions, to gain insight into the effects of shale composition on methane sorption. This was significantly higher in solvent-extracted samples than in raw samples, indicating that residual bitumen largely restricts methane sorption on such shales. A positive correlation between the amount of clay minerals and methane sorption capacity of bulk rocks was evident, suggesting that clay mineral content is relevant to methane sorption. This result was also supported by the much higher methane sorption capacity of solvent-extracted shales compared to the extracted kerogen from those shales, when measured sorption data was normalized to TOC values. The effects of both residual bitumen and clay mineral on the methane sorption of bulk rocks have complicated the evaluation of methane sorption on organic matter in these mature shales.

1. Introduction

Successful exploration and production of shale gas in USA has greatly encouraged investigations into the composition (both organic and inorganic) and the gas potential of shales from North America and Europe in the past ten years (Bowker, 2007; Chalmers and Bustin, 2007a, 2008a,b; Curtis, 2002; Gasparik et al., 2014; Hammes et al., 2011; Jarvie et al., 2007; Montgomery et al., 2005; Rexer et al., 2013, 2014; Ross and Bustin, 2007, 2008, 2009; Selley, 2012; Strąpoć et al., 2010). In the past few years, Chinese geologists have shown increasing interest in the composition and gas potential of shales (Chen et al., 2011; Han et al., 2013; Wang et al., 2013), and shale gas was licensed as a new type of mineral resource by the Chinese Government in 2011 to accelerate the exploration of shale gas. The reported results from China have exclusively focused on the very old marine shales from South China, e.g. very high-maturity Cambrian and Silurian strata (mostly VRo > 2.0%). Permian, Triassic, Jurassic, and Cretaceous to Paleocene lacustrine shales containing very abundant organic matter are widespread in northern China. These have contributed greatly to

* Corresponding author. Tel.: +86 20 85291312; fax: +86 20 85290706.
E-mail address: wljia@gig.ac.cn (W. Jia).

http://dx.doi.org/10.1016/j.marpetgeo.2014.05.010
0264-8172/

petroleum production in China (Duan et al., 2008; Gong et al., 2010; Tang et al., 2010; Zou et al., 2013). They are generally less mature than the marine shales.

Shale gas is stored differently depending on three types of geological environment: free gas in pores and/or fractures, gas sorbed onto kerogen and clay minerals and, to a lesser extent, gas dissolved in residual bitumen (Curtis, 2002). Isotherm sorption of methane onto shales under high-pressure conditions, and the relationship between shale composition and sorbed methane capacity, have been extensively studied to determine the gas potential of shales. The percentage of sorbed gas in the total gas varies greatly (Chalmers and Bustin, 2007a; Lu et al., 1995; Montgomery et al., 2005; Ross and Bustin, 2008). Positive correlations between the amount of organic matter and the sorbed methane capacity have frequently been reported (Chalmers and Bustin, 2007a, 2008a; Chen et al., 2011; Gasparik et al., 2014; Han et al., 2013; Lu et al., 1995; Ross and Bustin, 2007, 2009; Zhang et al., 2012).

These have suggested that organic matter exerts primary control over sorbed gas, but also indicated the significant effects of organic matter on the pore structure of shales (especially pores at the nanoscale) (Curtis et al., 2012; Loucks et al., 2009; Rexer et al., 2014; Ross and Bustin, 2007, 2009; Slatt and O'Brien, 2011; Valenza et al., 2013). The type of organic matter also affects the sorbed methane capacity. It is higher for type II/III kerogen, when normalized to the organic matter content, than for type I/II kerogen (Chalmers and Bustin, 2008a). Zhang et al. (2012) further suggested that kerogens with mainly aromatic structures adsorbs methane more readily than with mainly aliphatic structures.

Relatively high-maturity shales have a higher capacity for sorbed methane than those of low maturity, for comparable organic matter and moisture contents (Gasparik et al., 2014; Jarvie et al., 2007; Ross and Bustin, 2007, 2009). This phenomenon might be related to the development of organic porosity in shales of elevated maturity (Curtis et al., 2012; Valenza et al., 2013). Some clay minerals, e.g. montmorillonite and illite, have abundant micropores and also a high methane sorption capacity (Ji et al., 2012; Liu et al., 2013; Lu et al., 1995; Ross and Bustin, 2009), and have been reported to contribute to the methane sorption on shales when measured on a dried basis (Chalmers and Bustin, 2008a; Gasparik et al., 2012; Rexer et al., 2014).

For shales of normal maturity, the residual bitumen filling the pores or pore throats (Jarvie et al., 2007; Ross and Bustin, 2009) complicates the evaluation of the effects of shale composition on methane sorption. After bitumen is extracted using an organic solvent, the surface area of mature shales increases (Valenza et al., 2013). A recent study (Guo et al., 2014) further suggested that removing the residual bitumen leads to a large increase in the sorption of N_2 and CO_2 on mature shales. As a result, the calculated surface areas and volumes both of the micropores and mesopores of bitumen-extracted shales were much higher than in shales where the residual bitumen has not been extracted. However, to date this effect has not previously been investigated for methane sorption on mature shales under high pressure.

Lacustrine shales from the Upper Triassic Yanchang Formation are some of the most important petroleum resources in China. Preliminary investigations have indicated a good gas potential (Wang et al., 2012), and detailed characterization is accordingly much needed. This study investigated the organic and mineral compositions of 41 core samples from the Yanchang Formation, collected from the south-eastern Yishan slope of the Ordos Basin (Fig. 1a). Ten bulk samples were selected for methane sorption analysis. A further three samples were chosen to demonstrate the effect of the composition of the shale on the methane sorption by mature shales, by comparing the methane sorptions of bulk rock and bitumen-extracted rock, and their corresponding kerogens.

2. Samples and experiments

2.1. Geological background and samples

The Ordos Basin in northern-central China (Fig. 1a) is the second largest sedimentary basin in China, with vast oil and gas reserves (Dai et al., 2005; Duan et al., 2008). It is an intracratonic depression basin covering an area of approximately 32×10^4 km^2 (Li, 1996) and is well known as one of the most tectonically stable basins in China (Dai et al., 2005). It comprises six major structural units (Duan et al., 2008): the Yimeng uplift in the north, the Weibei uplift in the south, the Tianhuan depression and western edge thrust belt in the west, the Jinxi fold belt in the east, and the central Yishan slope (Fig. 1a). The Ordos Basin is a large asymmetrical syncline with a broad, gently dipping eastern limb and a narrow, steeply dipping western limb. The Tianhuan Sag forms the axis of the syncline (Ding et al., 2013). The Yishan slope, which covers the largest area of the Ordos Basin, dips at less than 1° toward the west. It is the main oil and gas exploration and production area in the basin. One main source unit is Upper Paleozoic strata (Dai et al., 2005) marked by Carboniferous–Permian coal measures; another is the lacustrine shales in the Yanchang Formation in Upper Triassic strata (Duan et al., 2008). Generally, most of the large conventional gas fields occur in the northern Yishan slope, and have been genetically related to the Carboniferous–Permian coal measures (Dai et al., 2005). Most of the oil fields in the basin occur in the Southern Yishan slope, with oil mainly originating from the Yanchang shales (Dai et al., 2005; Duan, 2012; Duan et al., 2008; Wang et al., 1995). The area has recently been targeted for shale gas exploration in terrestrial strata, and the Yan'an region (Fig. 1a) was selected in 2012 as a national demonstration zone for shale gas in China. The first vertical well and the first horizontal well in this area, specifically for gas exploration from terrestrial shales, were drilled in 2011 and 2012, respectively, and hydraulic fracturing was also carried out.

The Yanchang shales, which are divided into 10 sections (Fig. 1b), result from the evolution of lake deposits in the Late Triassic (Yao et al., 2009). Sections Chang 9 and Chang 10 were deposited during the genetic and expanding stage of the lake basin, which later reached its peak stage. Chang 7 developed rapidly once this peak stage had been reached. During the deposition period of the Chang 4, 5 and 6 sections, the area and depth of the lake basin significantly decreased. The lake basin subsequently evolved into its final stage, and Chang 1, 2 and 3 sections were mainly deposited in the resulting deltaic environment. Oil shale, black shale and carbonaceous shale are very common in semi-deep and deep-lake conditions in the Chang 7 section, and petroleum resources have been well correlated with the shales in this section, which contains abundant organic matters (Duan et al., 2008; Zhang et al., 2009). The Chang 9 shales also have a very high potential for oil generation (Zhang et al., 2007). In the present study, shale samples from the Chang 7 and 9 sections were collected from 20 wells drilled in the south-eastern Yishan slope (Fig. 1a, Table 1). These are denoted Chang 7 and Chang 9 shales for the convenience of discussion in this context.

2.2. Experimental analysis

2.2.1. Geochemical analysis

Shale cores were crushed and −200 mesh material samples were selected for geochemical analysis. About 100 mg was placed in a crucible with 5% HCl at 80 °C to remove carbonates. A Leco C230 carbon analyzer measured the total organic carbon content (TOC in Table 1). A Vinci Rock Eval 6 instrument determined the type, maturity and hydrocarbon generation potential of the organic

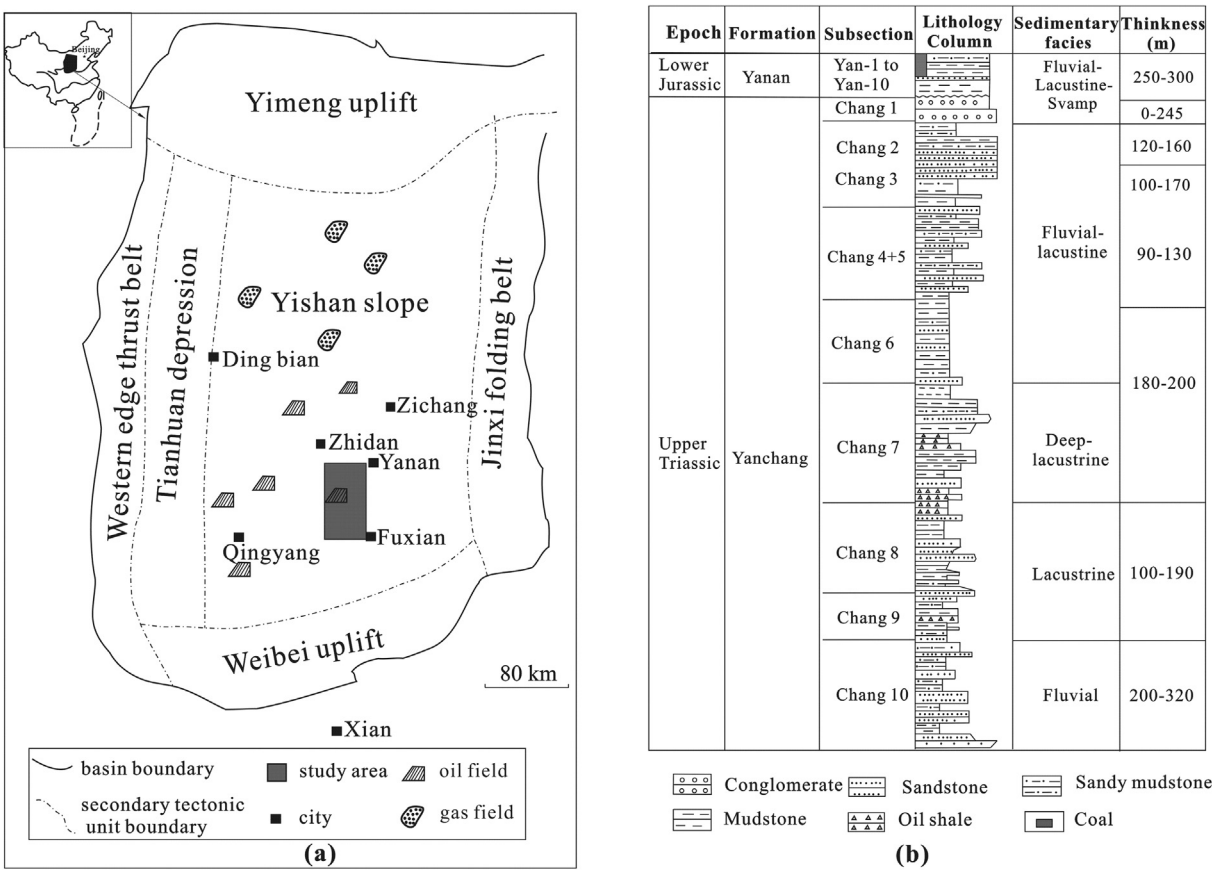

Figure 1. (a) Simplified structural map of the Ordos Basin showing the location of conventional gas and oil fields; (b) Upper Triassic and Lower Jurassic stratigraphy and depositional environment (modified after Dai et al., 2005 and Duan et al., 2008).

matter in a sample weighing about 70 mg. Soxhlet extraction was applied to about 20 g of the sample using a 25:2 vol/vol mixture of dichloromethane and methanol for 72 h, and the extracted mixture was concentrated in a rotary evaporator. The extracted organic matter (EOM) concentrate was weighed in a 4 cm^3 glass vial (Table 1).

2.2.2. Analysis of kerogens isolated from shales

The kerogen fraction was prepared by the standard procedure: the rock powder was treated with hydrofluoric and hydrochloric acid and the isolated kerogen powder was further purified by Soxhlet extraction using a 25:2 vol/vol dichloromethane/methanol mixture. A Leica MPV-SP microphotometer then determined the maceral content of the purified kerogen and the mean random reflectance of vitrinite content (VRo).

The elemental composition of the kerogen powder was determined using a Elementar vario EL III elemental analyzer. The C, H, N and O contents were measured by combustion (950 °C) and pyrolysis (1100 °C). The isotopic composition of the carbon in the kerogen was measured on a Finnigan™ DELTAplusXL isotope ratio mass spectrometer (IRMS) coupled to a CE Elantech EA Flash-1112 elemental analyzer via a ConFlo III continuous-flow interface. The precision of the isotopic analysis was better than 0.2‰ (±one standard deviation, 1σ). Each sample was analyzed twice. The average value for the two analyses was taken as the final result for that sample.

2.2.3. Mineralogical composition determination by XRD

The mineralogy of the shale sample was determined by quantitative X-ray diffraction (XRD) analysis of powder finer than 200 mesh (i.e., <75 μm), following the two independent processes of the CPSC procedure (China Petroleum Standardization Committee, 2010). First, the bulk mineral composition of the powder sample was determined, at this stage including only the total clay content. Second, the individual clay mineral content of clay fractions separated from the rock powder sample was determined. The mineral composition was meaured by a Rigaku D/Max-RB diffractometer (Cu Kα radiation ($\lambda = 0.15418$ nm), 40 kV, 100 mA). A scan rate of 4° (2θ)/min was used in the range 5°–45° to record XRD traces. The two processes use the same instrument and measurement conditions.

2.2.4. High-pressure methane sorption

About 15 g of rock powder sample or 5 g of kerogen were analyzed for their methane sorption isotherms using the procedure reported by Wang et al. (2013), using a Sieverts PCT-Pro E&E gas sorption/desorption instrument (HY Energy Company Ltd.). Before analysis, bulk samples finer than 80 mesh were dried in an oven at 60 °C for 24 h. The working pressure of the gas reservoir was set in the range 0–12 MPa. The sample cell temperature was set at 50 ± 0.2 °C. The methane sorption capacity was determined for standard temperature and pressure conditions (0 °C, 101.325 KPa). The temperature and pressure applied in the sorption measurements were suitable for most collected samples under geological conditions (Table 1). For comparison, sorption isotherms were also determined for bitumen-extracted and kerogen samples under the same conditions.

2.2.5. Low pressure carbon dioxide isotherm sorption

A 3–4 g sample finer than 80 mesh was degassed for 12 h at 60 °C to remove moisture and some residual gas, then carbon

Table 1
Basic geochemical information and Langmuir fitting parameters for investigated Chang 7 and Chang 9 shales.

Sample[a]	Well	Depth (m)	TOC (%)	S1 (mg/g)	S2 (mg/g)	Tmax (°C)	HI (mg/g OC)	OI (mg/g OC)	EOM (%)	V_L (ml/g)	P_L (MPa)
C7-1	X-1	846.16	0.3	0.03	0.09	459	50	–	–	–	–
C7-2	X-2	1032.37	1.45	0.89	2.43	447	161	–	0.31	–	–
C7-3	X-3	772.40	0.43	0.06	0.2	455	59	32	–	–	–
C7-4	X-4	844.60	3.04	1.08	6.38	447	188	–	0.38	–	–
C7-5	X-5	1505.98	2.78	2.14	5.59	442	184	1	0.58	1.18	3.2
C7-6	X-6	1736.36	7.2	9.62	23.44	441	255	1	1.72	–	–
C7-7	X-7	1226.77	2.42	1.98	5.31	441	200	2	0.41	–	–
C7-8	X-8	1189.75	3.42	2.71	6.58	444	158	3	0.72	–	–
C7-9	X-9	978.38	3.56	1.65	9.02	449	227	1	0.51	–	–
C7-10	X-10	1004.32	2.07	0.61	3.17	448	144	–	–	–	–
C7-11	X-11	1315.10	5.74	4.56	14.71	442	199	–	0.92	–	–
C7-12	X-12	1140.03	3.7	3.55	8.02	436	202	4	0.66	1.87	4.4
C7-13	X-12	1149.74	4.25	4.77	11.63	434	230	–	0.71	0.8	1.4
C7-14	X-12	1148.02	3.65	5.95	9.1	442	197	–	–	–	–
C7-15	X-12	1155.23	4.21	3.94	8.29	424	185	3	–	–	–
C7-16	X-12	1146.11	4.08	5.09	11.79	437	249	1	–	–	–
C7-17	X-12	1153.19	4.33	3.79	9.47	435	190	7	–	–	–
C7-18	X-12	1142.98	4.79	4.39	11.42	448	219	2	–	–	–
C7-19	X-13	1519.91	5.46	2.68	9.34	450	151	1	0.62	0.65	1.4
C7-20	X-13	1514.85	2.39	2.59	4.28	441	170	4	–		
C7-21	X-13	1522.88	3.58	3.13	6.42	425	167	13	0.73	1.8	4.7
C7-22	X-13	1531.33	5.88	3.37	11.17	443	173	3	–	–	–
C7-23	X-13	1526.72	5.4	3.4	10.47	437	167	5	–	–	–
C7-24	X-14	731.08	1.92	1.08	2.76	449	149	8	0.38	–	–
C7-25	X-15	1846.62	7.68	3.88	15.16	448	180	1	1.12	2.04	3.2
C9-26	X-1	1117.84	1.6	0.42	1.66	466	114	4	–		
C9-27	X-2	1124.28	2.02	0.42	1.92	465	97	–	0.35	1.73	4.3
C9-28	X-16	912.52	2.96	1.1	3.73	453	121	–	0.35	–	–
C9-29	X-17	1586.60	5.35	3.16	8.07	449	141	–	0.75	–	–
C9-30	X-19	1179.89	2.06	1.78	4.68	429	227	–	0.53	–	–
C9-31	X-11	1500.90	5.79	2.69	7.48	454	114	4	0.64	2.15	3.4
C9-32	X-18	1402.33	9.74	1.96	15.35	458	174	–	0.88	1.82	1.2
C9-33	X-20	1528.22	6.52	2.36	9.54	457	134	1	0.69	–	–
C9-34	X-12	1302.52	6.31	3.31	10.32	451	140	–	–	–	–
C9-35	X-12	1306.34	8.39	3.71	13.26	456	143	–	0.88	–	–
C9-36	X-12	1303.14	6.22	3.19	10.17	449	148	–	–	–	–
C9-37	X-12	1308.11	4.65	3.12	8.19	449	158	–	0.73	–	–
C9-38	X-12	1304.84	7.65	3.71	13.3	454	154	–	–	–	–
C9-39	X-12	1300.42	5.73	2.86	9.4	451	129	–	–	–	–
C9-40	X-12	1301.69	4.57	2.56	8	449	149	–	–	–	–
C9-41	X-21	1211.19	2.28	1.07	5.01	436.5	234	4	0.51	1.51	3.5

[a] C7 and C9 are short for Chang 7 and Chang 9 respectively; V_L, the Langmuir volume of sorbed gas; P_L, the Langmuir pressure at which the volume of sorbed gas reach one-half of V_L. Geochemical data of two samples (C7-19 and C9-32), including TOC values, pyrolysis parameters and EOM values, were reported in Guo et al. (2014).

dioxide sorption analysis was performed at 0 °C to determine the surface area and volume of micropores whose diameter was less than 2 nm using a Quantachrome NOVA 4200e analyzer. The surface area of the micropores was determined from the Dubinin–Radushkevich (D–R) equation (Gregg and Sing, 1982) assuming the cross-sectional area of a CO_2 molecule is 0.2 nm^2. The micropore volume was determined using nonlocal density functional theory (NLDFT) (Vishnyakov et al., 1999).

3. Results and discussion

3.1. Geochemical characteristics

In the study area, both Chang 7 and Chang 9 shales contained abundant organic matter (Table 1). The average TOC was 3.7% ($n = 25$) for Chang 7 shale and 5.1% ($n = 16$) for Chang 9 shale. A large database of Lower Cretaceous gas shales from Northern British Columbia, which were mainly immature and mature, showed a trend of decreasing TOC with increasing Tmax (the temperature at peak evolution of S2 hydrocarbons from Rock-Eval pyrolysis) for shales containing various types of organic matter (Chalmers and Bustin, 2008a). However, the TOC values of both Chang 7 and Chang 9 shales displayed little variation with elevated maturity level as indicated by the Tmax values of bulk rocks (Fig. 2a).

3.1.1. Types of organic matter

Based on Rock-Eval data, most Chang 7 and 9 shales followed the trend line for type II_2 organic matter; however, several samples of Chang 9 deviated from this trend line. These may have contained types I or II_1 organic matter (Fig. 2b), which would be consistent with the maceral compositions of several of the kerogens isolated from shale samples (Fig. 3a). In all the kerogens investigated in this work, amorphinite macerals were observed only in the liptinite group, which generally made up 50–80% of the organic macerals in total. Most Chang 7 kerogens contained more vitrinite and inertinite than Chang 9.

The elemental ratios of isolated kerogen fractions suggest contributions from type III organic matter to both Chang 7 and 9 (Fig. 3b). The relatively high O/C atomic ratios in a few of the kerogens may be related to the inorganic residuals in the isolated kerogen, as indicated by the relatively low carbon content in these kerogens (Table 2). Nine kerogen samples showed limited variations in $\delta^{13}C$ values, in the range −28.5‰ to −30‰, similar to the carbon isotopic compositions of organic matter in Barnett shales from Texas (Rodriguez and Philp, 2010). The kerogen isolated from

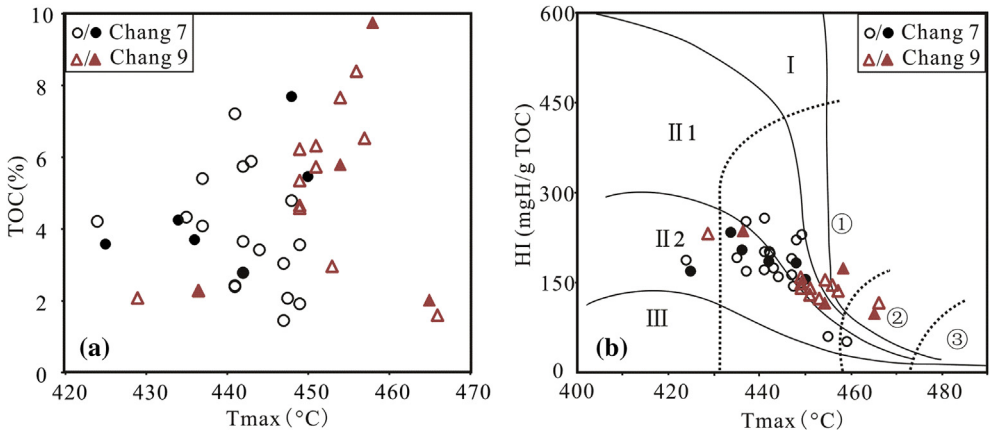

Figure 2. (a) Plot of TOC versus Tmax for Chang 7 and Chang 9 shales; (b) Plot of hydrogen index (HI) versus Tmax, showing the types of organic matter and maturity levels of shale samples. Filled symbols denote samples selected for methane adsorption measurements. Labels ①, ② and ③ in Fig. 2b denote oil window, wet gas window and dry gas stage, respectively.

shale sample C9-32, which was significantly richer in ^{13}C ($\delta^{13}C$ values −27‰), might also suggest the possibility of type III organic matter.

3.1.2. Maturation

According to the Rock-Eval database, Chang 7 and 9 shales are mainly in the oil window at the present time (Fig. 2b). Two Chang 7 samples might be immature, and two Chang 9 shale samples have evolved to the condensate-wet gas stage. This result was supported by the vitrinite reflectance (VRo) of the extracted kerogen fractions, which mainly ranged from 0.7% to 1.2% (Table 2). The relatively high content of residual bitumen in the bulk rocks (0.3%–1.2%, EOM in Table 1) indicates that these shales are also currently in the oil window. With the exception of two samples, Tmax and VRo were higher in Chang 9 than in Chang 7 (Fig. 2b; Table 2). Therefore, Chang 7 shales are generally at the start and peak of the oil window, while Chang 9 shales are at the late stage of the oil window and at the early condensate stage. Jarvie et al. (2007) proposed that shales with relatively low Ro and Tmax values (Ro < 1.0% and Tmax < 455 °C) had very low potential for gas flow rates. From the view point of maturity, Chang9 shales seem to have higher gas potential than Chang7 shales.

3.1.3. Amount of residual bitumen

The amount of residual bitumen in the source rocks was evaluated in two ways. One was based on the S1 obtained from the Rock-Eval analysis; the other was by quantifying the EOM in the source rocks using organic solvents. The EOM values for most of the Chang 7 and Chang 9 shale samples exhibited good positive correlation with S1 values obtained from the Rock-Eval analysis; however, they were generally double the S1 values (Fig. 4a). This might be related with the fact that some high molecular weight organic matter, e.g. partial resins and asphaltenes, were not included in the S1 values due to their relatively high stability and boiling point. Experimental simulation and kerogen swelling data has indicated that oil expulsion results in richer resins and asphaltenes in the residual bitumen than in the expelled oil (Kelemen et al., 2006a; Lafargue et al., 1990, 1994; Ritter, 2003; Sandvik et al., 1992). Delvaux et al. (1990) used the comparative Rock-Eval analysis of solvent-extrated and unextracted rocks to allow a better estimating of total bitumen content based on the pyrolysis data. EOM values indicate that the amount of residual bitumen in Chang 7 and Chang 9 shales was well positively correlated with TOC (Fig. 4b), which suggests that the solid organic matter in shales, i.e. kerogen, controls the amounts of residual

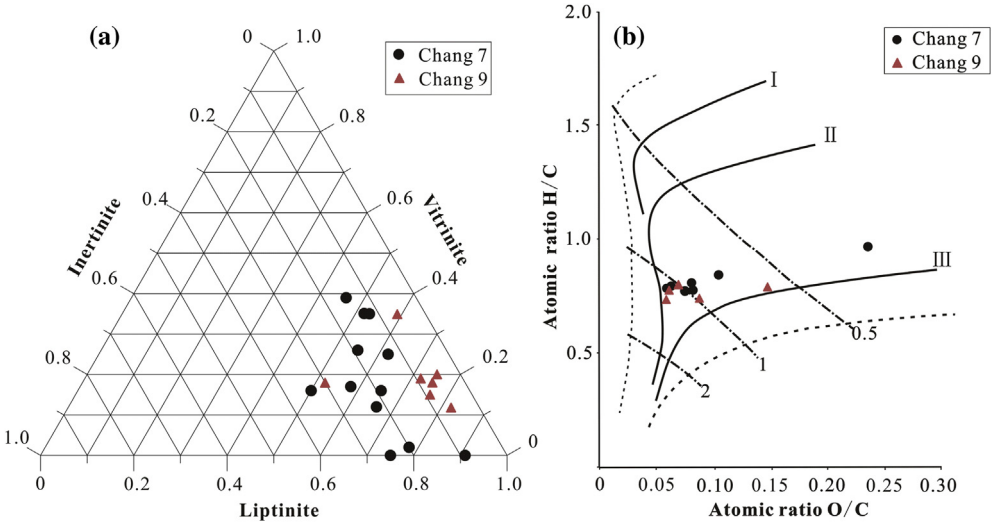

Figure 3. (a) Ternary diagrams of maceral composition of kerogens isolated from Chang 7 and Chang 9 shales. (b) Plot of H/C atomic ratio versus O/C atomic ratio of the isolated kerogens. Numbers (0.5, 1 and 2) in Fig. 3b show the Ro values.

Table 2
Maceral, elemental and carbon isotopic compositions of kerogens isolated from Chang 7 and Chang 9 shales.

Sample	Liptinite (%)	Vitrinite (%)	Inertinite (%)	VRo (%)	N (%)	C (%)	H (%)	O (%)	H/C	O/C	$\delta^{13}C$ (‰)
C7-2	78	2	20	0.72	–	–	–	–	–	–	–
C7-8	50	16	34	0.62	–	–	–	–	–	–	–
C7-9	91	–	9	–	–	–	–	–	–	–	–
C7-11	75	–	25	–	1.21	37.80	3.05	11.89	0.97	0.24	−29.3
C7-12	66	12	22	0.81	2.74	77.52	5.11	6.30	0.79	0.06	−28.7
C7-13	55	26	19	0.94	2.61	73.68	4.76	5.47	0.78	0.06	−29.0
C7-17	52	35	13	0.78	–	–	–	–	–	–	–
C7-18	58	17	25	–	1.96	59.63	4.22	8.34	0.85	0.10	−28.7
C7-19	65	16	19	1.09	2.76	71.70	4.92	7.54	0.82	0.08	−29.3
C7-21	46	39	15	1.09	2.46	68.27	4.47	7.44	0.79	0.08	–
C7-24	53	35	12	0.78	–	–	–	–	–	–	–
C7-25	62	25	13	1.01	2.32	66.98	4.34	6.72	0.78	0.08	−29.3
C9-26	75	18	7	1.14	–	–	–	–	–	–	–
C9-30	76	15	9	–	1.84	70.07	4.56	5.68	0.78	0.06	–
C9-31	82	12	6	1.17	1.62	51.85	3.42	10.22	0.79	0.15	−29.9
C9-32	72	19	9	1.17	2.38	76.67	5.11	7.56	0.80	0.07	−27.0
C9-35	75	20	5	1.10	1.37	45.89	2.83	5.37	0.74	0.09	−30.0
C9-37	52	18	30	1.28	1.64	59.44	3.65	4.64	0.74	0.06	−30.4
C9-39	59	35	6	1.12	–	–	–	–	–	–	–

VRo values of two samples (C7-19 and C9-32) have been reported in Guo et al. (2014).

bitumen in their source rocks, mainly by adsorption or absorption (Kelemen et al., 2006b; Pepper and Corvi, 1995; Ritter, 2003; Sandvik et al., 1992).

3.2. Mineralogy

Chang 7 and 9 shales possessed similar mineral compositions: most abundant were silica minerals (quartz and feldspars) and clay minerals; carbonates generally were less than 10% (Fig. 5; Table 3). Quartz and feldspars ranged from 40% to 80% (average 58%, $n = 25$); clay minerals ranged from 20% to 60% (average 36%). The quartz content (20–50%, average 35%) was generally higher than feldspar content. Compared with summarized mineralogical data of various gas shales worldwide (Han et al., 2013), the mineralogical composition of Chang 7 and 9 shales was similar to Ohio shales, Woodford/Barnett shales (western Texas) and Lower Cambrian shales from Northern Guizhou in China. An illite/smectite mixed-layer mineral is the dominant clay mineral in both shales (Table 3). Illite is generally the most abundant clay mineral in other gas shales (Chalmers and Bustin, 2008a; Han et al., 2013; Ross and Bustin, 2007, 2008). The dominance of mixed layers of illite and smectite has been observed for black shales in The Netherlands (Gasparik et al., 2012) and in Upper Carboniferous and Lower Permian shales from the Ordos Basin in China (Ding et al., 2013). The mineralogy can greatly affect the brittleness of shales (Jarvie et al., 2007). The average clay mineral content of the primary producing facies of the Barnett shale is 27% (Montgomery et al., 2005), and high clay contents of shales will challenge the fracking techniques (Ross and Bustin, 2008).

3.3. Methane sorption on bulk rocks and isolated kerogens at 50 °C

Methane sorption isotherms for the Chang 7 and Chang 9 shales show large variations, and are well fitted by the Langmuir equation (Fig. 6). Six Chang 7 shales with 2–8% TOC showed large variations in maximal methane sorption capacity (0.6–2 cm^3/g). Four Chang 9 shales, with comparable TOC values (2–10%) varied less (1.5–2.2 cm^3/g, Table 1). There have been numerous reports on the methane sorption capacity of gas shales worldwide (Chalmers and Bustin, 2007a, 2008a; Chen et al., 2011; Gasparik et al., 2012, 2014; Lu et al., 1995; Ross and Bustin, 2007, 2009; Wang et al., 2013; Zhang et al., 2012).

The temperature at which measurements were made greatly influenced methane sorption capacity; therefore, four immature to over-mature gas shales for which methane sorption was determined at 50 °C on a dried basis (Zhang et al., 2012), as in the present work, were selected for comparison. The methane sorption volume of Chang 7 and Chang 9 shales at 12 MPa (0.5–1.7 cm^3/g, Fig. 6a) was much lower than that of Woodford shale and Green River shale (Colorado), which both have very high TOC values (methane

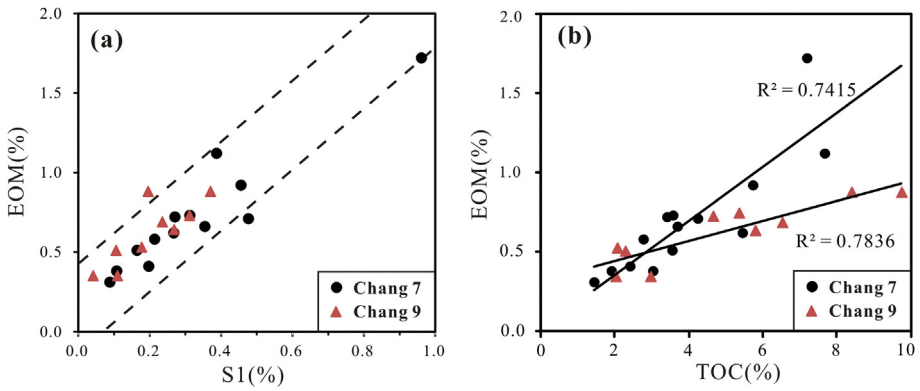

Figure 4. Relationship for Chang 7 and Chang 9 shales between (a) EOM and S1; (b) EOM and TOC. S1 denotes free hydrocarbons in the Rock-Eval analysis (Table 1).

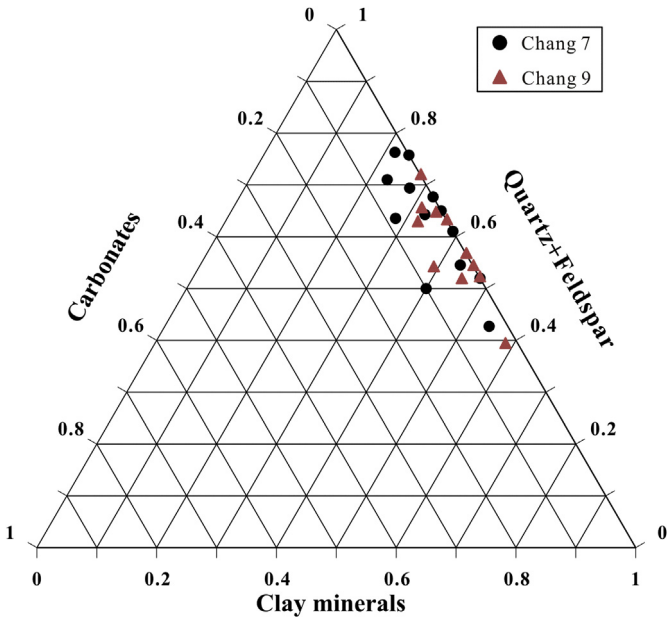

Figure 5. Ternary diagram of mineral compositions of Chang 7 and Chang 9 shales.

sorption volume 2.6–2.9 cm^3/g, TOC 17.2% and 20.7%, Table 3 in Zhang et al., 2012). Three Barnett shales with TOC values of 6–8% also showed a higher methane sorption volume (2.0–2.2 cm^3/g, Table 3 in Zhang et al., 2012) than some of the Chang 7 and Chang 9 shales that contained abundant organic matter (about 1.6 cm^3/g, samples C7-25 and C9-32 with TOC 7–10%, Fig. 6a).

The effect of the degassing temperature prior to sorption measurement might be one possible explanation. The degassing temperature in the present work was 60 °C, to eliminate the loss of residual bitumen in mature shales; this had also been done in some previous studies (Valenza et al., 2013; Wang et al., 2013). A relatively high temperature (200 °C, Zhang et al., 2012) was used to completely remove the moisture and gas in the shales. Notably, two samples of Chang 7 shale with the relatively high TOC values of 4.25% and 5.46% showed a much lower methane sorption capacity than three samples with lower TOC. The methane sorption capacity of Chang 9 samples was generally higher than for Chang 7 samples with comparable TOC values.

It seems likely that other factors have affected the relationship between TOC and methane sorption capacity for these mature shales. The methane sorption volume at 12 MPa for three kerogen samples from Yanchang shales (8.5–12 cm^3/g TOC, Fig. 6b) was much lower than for Green River kerogen (about 15 cm^3/g TOC) and Woodford kerogen (about 21 cm^3/g TOC), Tables 2 and 4 in Zhang et al., 2012. The carbon content of isolated kerogen samples in the present work ranged from 71% to 77% (Table 2), slightly above those of Green river kerogen (63.9%) and Woodford kerogen (69.6%). Therefore, it is possible that inorganic mineral content has a minor influence.

3.4. Influence of residual bitumen on methane sorption of mature gas shales

Significant amounts of residual bitumen (mostly 0.3–1.2% by weight, Table 1, Fig. 4) and of total organic matter (mostly 10–25%) remain in the rock mass after oil has been expelled from mature shales. Residual bitumen is closely bonded with kerogen by adsorption or absorption (Pepper and Corvi, 1995; Thomas and Clouse, 1990); therefore it would be expected that residual bitumen would have a large effect on the chemical and physical properties of gas shales, and on their methane sorption capacity. In the present work, the methane sorption under high-pressure conditions was compared for both bitumen-extracted and unextracted shales. Three shale samples with different TOCs and at different maturity levels were selected and extracted using the dichloromethane/methanol. Their methane sorption isotherms are shown in Figure 7 along with those of the original shale samples. Although residual bitumen was present in a small percentage of the bulk shales (usually less than 1% by weight, Table 1, Fig. 4), the extraction of bitumen from three samples led to a large increase in the methane sorption volume of the bulk rock (Fig. 7). The

Table 3
Mineralogical composition of selected Chang 7 and Chang 9 shale samples (%).

Sample	Quartz	Feldspar	Total clays	I/S	Illite	Kaolinite	Chlorite	Carbonates	Pyrite
C7-2	33	34	32*	–	–	–	–	–	–
C7-4	38	25	32*	–	–	–	–	3	1
C7-5	39	36	24	20	1	–	3	–	1
C7-6	42	19	27*	–	–	–	–	8	4
C7-7	47	27	21*	–	–	–	–	2	3
C7-10	31	34	35*	–	–	–	–	–	–
C7-11	36	22	37	33	2	–	2	–	5
C7-12	26	26	48	41	3	–	4	–	1
C7-13	39	29	27	18	2	3	4	3	1
C7-19	27	27	43	27	4	6	6	2	2
C7-21	30	20	40	34	3	–	3	10	2
C7-24	36	35	23*	–	–	–	–	6	–
C7-25	28	13	52	42	4	–	6	3	4
C9-26	40	23	37*	–	–	–	–	–	–
C9-27	42	10	48	43	1	–	4	–	–
C9-28	31	31	32*	–	–	–	–	5	1
C9-29	35	29	31*	–	–	–	–	3	4
C9-30	35	23	35	27	3	–	5	6	1
C9-31	31	17	42	37	2	–	3	3	6
C9-32	32	28	40	34	2	2	2	–	1
C9-33	23	13	54*	–	–	–	–	2	8
C9-35	38	15	35	30	3	–	2	2	9
C9-37	44	8	44	41	1	–	2	–	4
C9-41	39	32	28	20	5	–	3	–	1

I/S, illite–smectite mixed layer mineral; *, only the total clay content is available, and the content of individual clay mineral was not determined. Mineral compositions of two samples (C7-19 and C9-32) were reported in Guo et al. (2014).

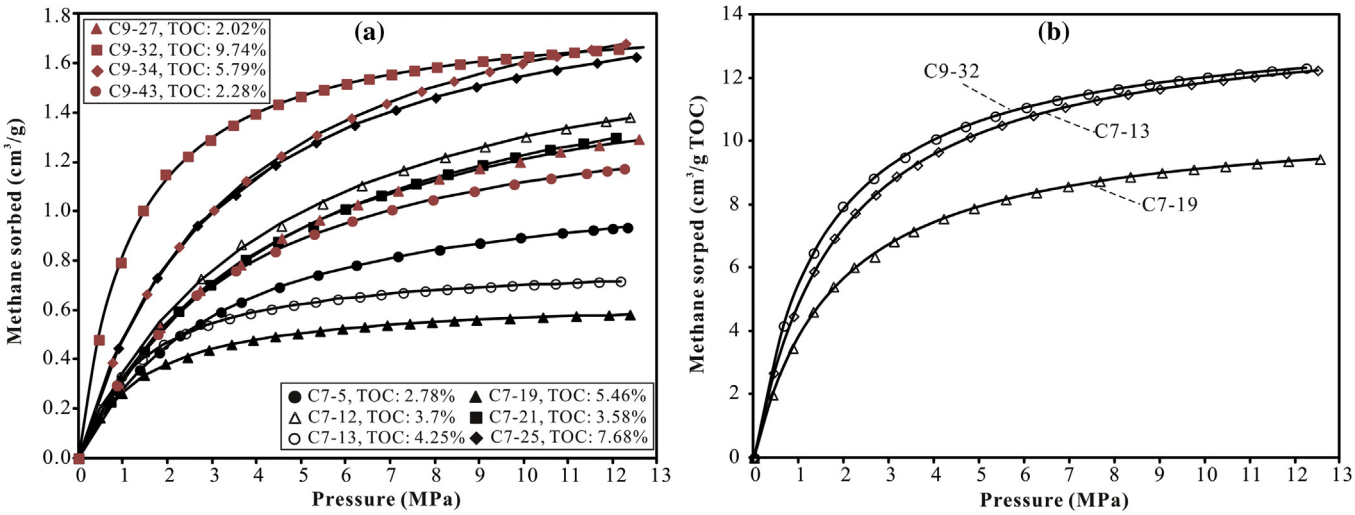

Figure 6. Methane sorption isotherms for Chang 7 and Chang 9 shales at 50 °C: (a) bulk rocks; (b) isolated kerogen. Lines are fitted Langmuir results.

maximum sorption capacity of the bitumen-extracted shales was double or more that of the untreated shales.

A recent study (Valenza et al., 2013) showed that dichloromethane/methanol bitumen extraction greatly increased both the surface area and micropore volume of various gas shales, as determined by the low pressure nitrogen method. This result suggests that residual bitumen occupies many sorption sites and micropores in the solid absorbents (kerogen and mineral). Previous studies showed that the methane sorption capacity was closely related to the micropores and low-pressure CO_2 adsorption at 0 °C has been used to characterize the micropores (Chalmers and Bustin, 2007a, 2008a; Ross and Bustin, 2008, 2009).

Low-pressure CO_2 sorption analysis has been conducted on the three sample pairs to confirm the increase in micropore surface area and volume in bitumen-extracted shale; the results for two of the sample pairs (C7-19 and C9-32) have been reported previously (Guo et al., 2014). One additional sample pair (C7-13) was analyzed in the present work. Combined CO_2 sorption isotherms for the three sample pairs are shown in Figure 8; the calculated micropore surface areas and volumes are listed in Table 4.

The sorbed volume of CO_2 of three unextracted samples at the highest pressure displays a large variation from 0.2 to 2.0 cm^3/g (Fig. 8a), which is consistent with the range of sorbed CO_2 volumes of two samples of New Albany shale (Illinois Basin, USA) with high TOC values (5.8% and 15.8%, Mastalerz et al., 2013). Two of the three samples in the present work showed similar pore distribution, but the third (sample C7-13) differed slightly. Generally, micropores of approximately 0.5 and 0.6 nm diameter were the most abundant, and others of about 0.3, 0.4 and 0.8 nm were also prevalent (Fig. 8b–c).

The sorbed CO_2 volume of the three bitumen-extracted shales was much higher than for the unextracted shales, and was similar to the variations in sorbed methane volume under high pressure (Fig. 8a). The large observed increases in micropore volume and surface area are given in Table 4. Micropores of diameter about 0.5 and 0.6 nm were the most abundant in the unextracted samples, which is similar to the bitumen-extracted samples discussed above (Fig. 8b–c). One notable difference, however, was the significant increase of micropores at around 0.8 nm in the two solvent-extracted samples C7-13 and C7-19 (Fig. 8c). The results from CO_2 sorption in this work were consistent with those reported for N_2 sorption by Valenza et al. (2013), who worked with shales with a large variation in maturity level (from low-mature to over-mature). The expulsion of generated hydrocarbons was closely related to the growth of nanopores in shales (Valenza et al., 2013). With more nanopores on which gas could be adsorbed, the methane sorption

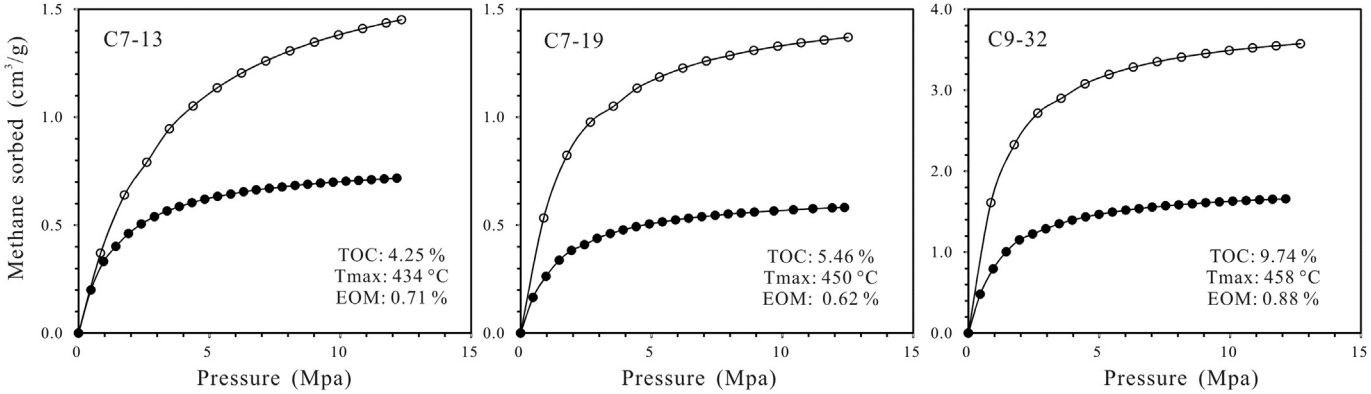

Figure 7. Methane sorption isotherms of three shale samples before and after bitumen extraction by organic solvents. The hollow and filled symbols denote the bitumen-extracted and original shale samples, respectively.

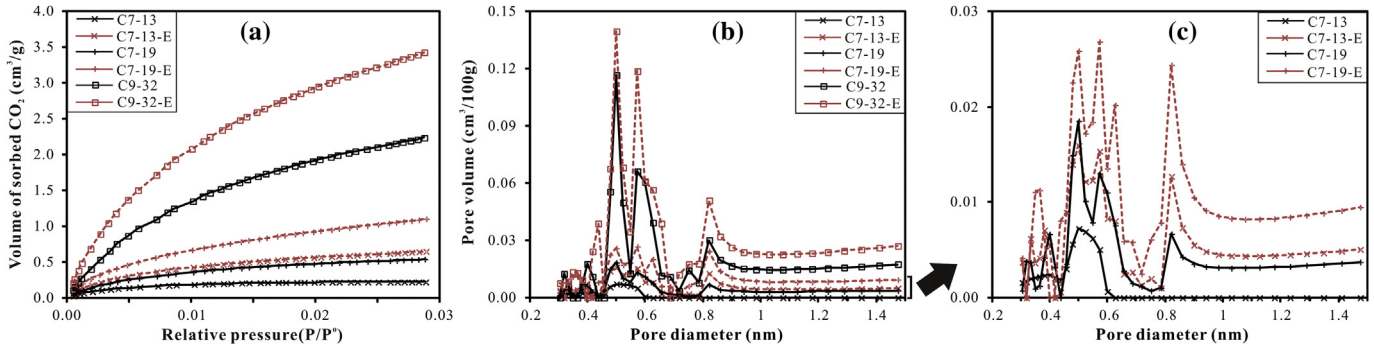

Figure 8. (a) Carbon dioxide sorption isotherms of three shale samples before and after extraction using organic solvents. (b), (c) Distribution of pore volume with diameter. C7-13-E, C7-19-E, C9-32-E are the respective extracted samples of C7-13, C7-19, C9-32.

capacity of bitumen-removed shales would be expected to be increased, as confirmed in the present work (Fig. 8).

3.5. Methane sorption by clay minerals in gas shales

Tests on the 10 samples of Chang 7 and 9 shales produced an ambiguous relationship between methane sorption capacity and organic matter content (Figs. 6a, 9a). Poor correlations between methane sorption capacity and TOC of gas shales have also been reported by Gasparik et al. (2012) and Ross and Bustin (2009). Inorganic minerals contribute to methane sorption in gas shales: experiments conducted under dry conditions on naturally occurring clay minerals have shown that montmorillonite and illite/smectite have a high sorption capacity for methane (Ji et al., 2012; Liu et al., 2013; Lu et al., 1995; Ross and Bustin, 2009). In the present work, two approaches were used to evaluate the extent to which the clay minerals in Chang 7 and 9 shales influence its methane sorption. One approach was to investigate how the sorption capacity of bulk shale rock was related to its clay content; the other was to compare the methane sorption of bulk rock with that of its kerogen.

Clay content was found to be positively correlated with methane adsorption in nine of the 10 samples (Fig. 9b). As stated above in Section 3.2, mixed layers of illite–smectite (I/S) dominated the clay minerals in these shales, and accordingly a positive relationship between methane sorption capacity and I/S was also evident (Fig. 9c). The other major minerals in Chang 7 and 9 were negatively correlated with methane sorption capacity (Fig. 9d). A positive correlation between it and total clay content in which I/S is the major mineral has been reported for black shales in The Netherlands (Gasparik et al., 2012). Chalmers and Bustin (2008a) suggested that clay minerals in Lower Cretaceous shales from north-eastern British Columbia had a significant effect on methane sorption on a dried basis, and organic matter content produced a notable influence in the methane sorption capacity of bulk rocks on a moisture-equilibrated basis. Therefore, the positive correlation between total clay content with methane sorption capacity in mature shales in the present study might be limited to results determined on a dried basis.

In order to evaluate the effects of minerals on the methane sorption of shales, it has been shown to be helpful to compare the methane sorption capacities of bulk rock samples and of their isolated kerogen fractions, after normalizing to their TOC values (Rexer et al., 2014; Zhang et al., 2012). In the present work, the three solvent-extracted gas shales and the kerogens they contained were compared for their methane sorption capacities (Fig. 10). Three bitumen-extracted shale samples were selected for the comparison, because of the large influences that the residual bitumen in these shales appeared to exert on the methane sorption of the bulk rock (Fig. 7). The kerogens were isolated from the shales after most of the residual bitumen had been removed. The methane sorption capacity of all three solvent-extracted rocks was found to be much higher than that of their kerogens; furthermore, the methane sorption capacity of the unextracted rocks was much higher than that of their kerogens, also (Fig. 10). This result suggests that methane sorption is related to both the clay mineral content and the kerogen.

Rexer et al. (2014) compared the methane sorption capacity of bulk Posidonia shales from The Netherlands and their kerogens, and estimated that about half of the methane sorption was related to organic matter. Although an earlier study had suggested that uncertainties in the TOC measurement procedure may lead to large errors in the normalized TOC sorption data in shale with relatively low organic matter content (Gasparik et al., 2012), the TOC of the shale in the present study was relatively high (4–10%), and it seems that the influence of TOC measurement uncertainty was minor.

Thus, clay minerals as well as solid organic matter contribute to the methane sorption capacity of bitumen-extracted Chang 7 and 9 bulk shales (measured on a dried basis). The predominance of the illite/smectite clay minerals in these shales might possibly be the reason for the positive correlation between clay mineral content and methane sorption capacity, since it has been shown that the methane sorption capacity of illite/smectite is relatively high. For example, the sorbed methane volume of an illite/smectite interstratified clay rock sample (approximately 50% quartz and 45% illite/smectite) has been reported to be in the order of 2.5 cm^3/g at 11 MPa and 50 °C (Table 2 in Ji et al., 2012).

The poor correlation between TOC and methane sorption capacity of the Chang 7 and 9 shales might also be related to the relatively low methane sorption capacity of their kerogens. The methane sorption capacity of immature Woodford and Green River shales is lower than that of their kerogens, which indicates that the kerogen exerts a major control over the methane sorption on gas

Table 4
Micropore volume and surface area of three selected samples and their solvent-extracted ones.

Sample	DFT volume (cm^3/100 g)	D–R surface area (m^2/g)
C7-13	0.1	2.39
C7-13-E	0.2	6.74
C7-19	0.2	6.09
C7-19-E	0.4	11.62
C9-32	0.7	29.58
C9-32-E	1.1	42.06

Data of two samples (C7-19 and C9-32) were reported in Guo et al. (2014).

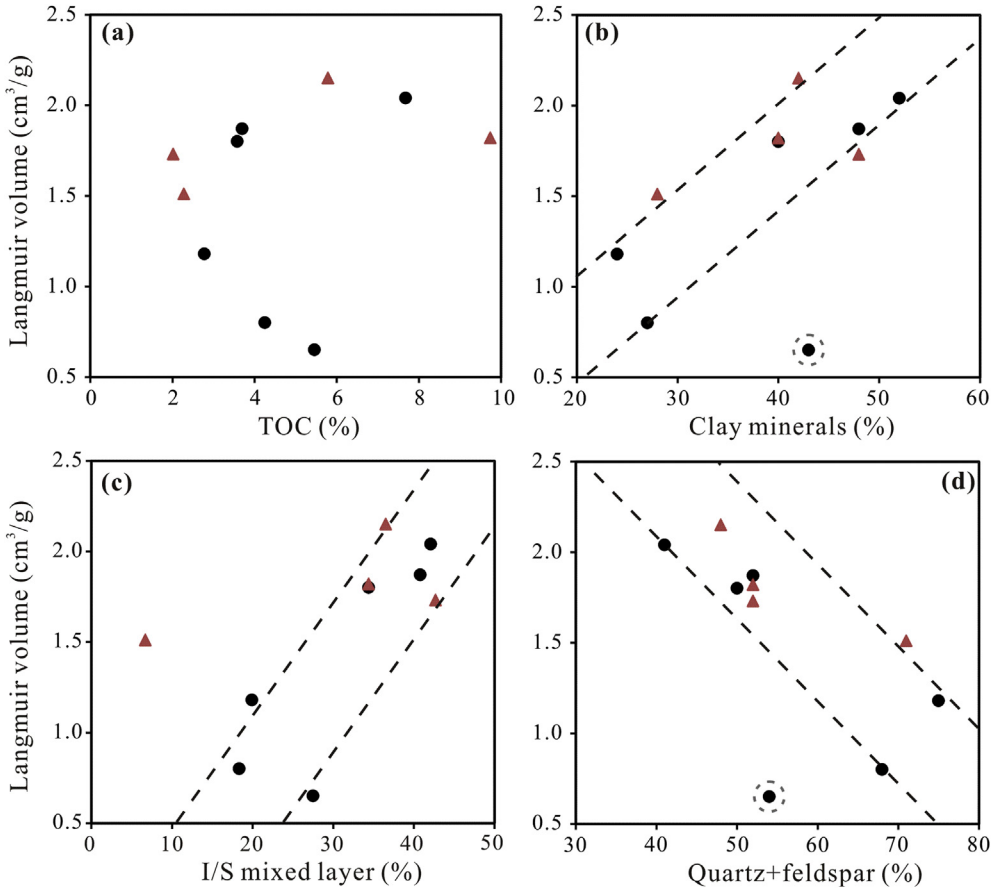

Figure 9. Variation of methane sorption capacity of Chang 7 and Chang 9 shales with amount of: (a) organic matter; (b) clay minerals; (c) I/S mixed layer; and (d) quartz and feldspar. Cycles and triangles denote Chang 7 and Chang 9 shales, respectively.

shales (Zhang et al., 2012). As stated above in Section 3.3, the methane sorption volume of the Woodford and Green River kerogens (about 21 and 15 cm^3/g TOC at 12 Mpa and 50 °C) is much higher than for the three kerogens in this study (8.5–12 cm^3/g TOC, Fig. 6b). Both the Woodford and Green River shales are low maturity shales containing types I and II organic matter, respectively. The three samples in the present work are from mature shales and mainly contain type II, with possibly some type III, organic matter. It has been well demonstrated that the methane sorption capacity of coal, usually containing type III organic matter, increases with coal rank (Chalmers and Bustin, 2007b; Clarkson and Bustin, 1996; Lamberson and Bustin, 1993; Prinz and Littke, 2005; Prinz et al., 2004; Yee et al., 1993).

Methane sorption by shales seems to be more complicated. Data for gas shales containing various types of organic matter shows that types II/III and III organic matter might produce a higher sorption capacity than types I and II (Chalmers and Bustin, 2008a; Zhang et al., 2012). The methane sorption capacities of the immature to over-mature Barnett shales vary only slightly (Zhang et al., 2012); likewise for black shales from The Netherlands (Gasparik et al.,

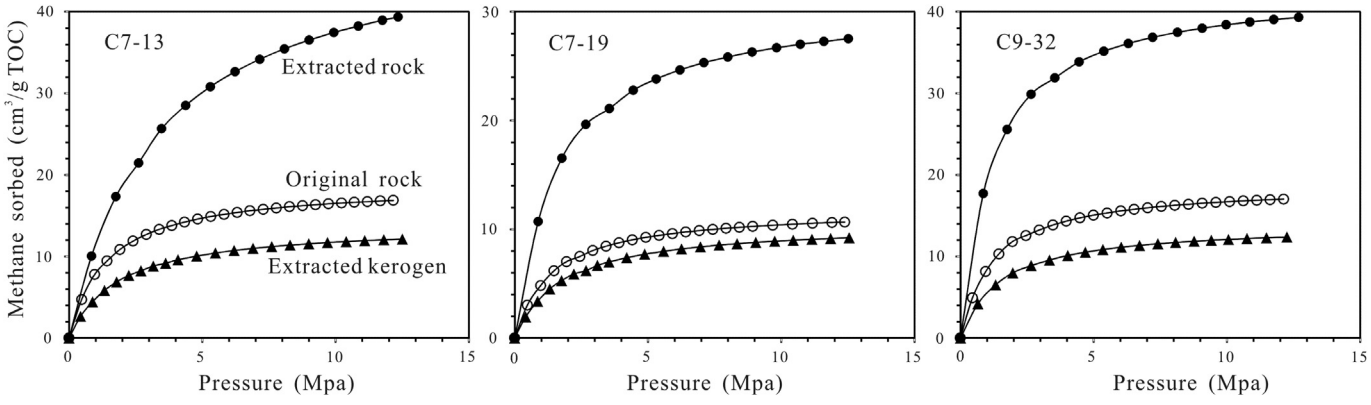

Figure 10. Comparison of methane sorption isotherms of bitumen-extracted rocks and their kerogen concentrates. Methane sorption isotherms of original rocks are also shown.

2012). Yet the methane sorption isotherms for shales at different maturity levels have shown obvious differences in both isotherm type and Langmuir constants (Gasparik et al., 2012; Zhang et al., 2012). However, high- to over-mature Devonian Mississippi shales generally have a much higher methane capacity (normalized TOC data) than mature Jurassic shales. This implies that the maturation process enhances the development of micropores and, thus, methane capacity (Chalmers and Bustin, 2008a; Gasparik et al., 2014; Ross and Bustin, 2009). Before any definitive assertions can be made about the geochemical factors that significantly influence methane sorption of the kerogen in gas shales, however, more kerogen samples need to be investigated to determine, for example, the type of organic matter and the maturity level.

4. Conclusions

Two sections of lacustrine shales (Chang 7 and Chang 9) from the Upper Triassic Yanchang Formation in the south-eastern Ordos Basin were investigated to determine their organic geochemical characteristics, mineralogy and methane sorption capacity on a dried basis. The methane sorption of the bitumen-extracted shales and their isolated kerogens were also measured to observe the effects of residual bitumen and clay minerals. Some preliminary conclusions are:

(1) Both Chang 7 and 9 shales had similar compositions, with abundant type II organic matter and major minerals quartz, clay minerals and feldspars. Mixed-layer illite/smectite dominates their clay minerals. Both shales are generally in the oil window; Chang 7 is slightly less mature than Chang 9. The methane sorption capacity of Chang 9 shales is 1.5–2.2 cm^3/g, generally higher than the 0.6–2 cm^3/g for Chang 7 shales, as determined on a dried basis at 50 °C. Therefore, those shales which have evolved into the wet gas window deserved to be studied in the future work.
(2) The methane sorption capacity of the bitumen-extracted bulk rocks is much higher than of the rocks retaining bitumen. This indicates that residual bitumen largely restricts methane sorption on these mature shales. Low-pressure CO_2 sorption analyses indicated that this phenomenon was related to the availability of fewer micropores for methane sorption in the unextracted shales.
(3) In addition to the organic matter, the relatively large amount of clay minerals in Chang 7 and 9 shales affects the methane sorption of bulk rocks under dried conditions. Evidence for this is the positive correlation between total clay content and methane sorption capacity of the bulk rocks, and the much higher methane sorption capacity of the solvent-extracted rocks than the extracted kerogens. However, relatively high clay contents in these shales could present some challenges for the production of shale gas.

Acknowledgments

This study was financially supported by the State “973” Project (2012CB214704), the Strategic Priority Research Programs (Category B) of Chinese Academy of Sciences (XDB10010200). The authors greatly appreciate the efforts of Dr. Zhiguang Song and Dr. Sibo Wang for the methane sorption analysis. We are grateful to two anonymous reviewers for their critical reviews that significantly improved the quality of the manuscript. The authors also thank Profs. O. Catuneanu and Xiaomin Zhu for handling of this paper. This is contribution No. IS-1913 from GIGCAS.

References

Bowker, K.A., 2007. Barnett shale gas production, Fort Worth Basin: issues and discussion. AAPG Bull. 91, 523–533.
Chalmers, G.R.L., Bustin, R.M., 2007a. The organic matter distribution and methane capacity of the Lower Cretaceous strata of northeastern British Columbia, Canada. Int. J. Coal Geol. 70, 223–239.
Chalmers, G.R.L., Bustin, R.M., 2007b. On the effects of petrographic composition on coalbed methane sorption. Int. J. Coal Geol. 69, 288–304.
Chalmers, G.R.L., Bustin, R.M., 2008a. Lower Cretaceous gas shales in northeastern British Columbia, part I: geological controls on methane sorption capacity. Bull. Can. Pet. Geol. 56, 1–21.
Chalmers, G.R.L., Bustin, R.M., 2008b. Lower Cretaceous gas shales in northeastern British Columbia, part II: evaluation of regional potential gas resources. Bull. Can. Pet. Geol. 56, 22–61.
Chen, S.B., Zhu, Y.M., Wang, H.Y., Liu, H.L., Wei, W., Fang, J.H., 2011. Shale gas reservoir characterisation: a typical case in the southern Sichuan Basin of China. Energy 36, 6609–6616.
Clarkson, C.R., Bustin, R.M., 1996. Variation in micropore capacity and size distribution with composition in bituminous coal of the Western Canadian Sedimentary Basin: implications for coalbed methane potential. Fuel 75, 1483–1498.
CPSC (China Petroleum Standardization Committee), 2010. Analysis Method for Clay Minerals and Ordinary Non-clay Minerals in Sedimentary Rocks by X-ray Diffraction. SY/T 5163–2010.
Curtis, J.B., 2002. Fractured shale-gas systems. AAPG Bull. 86, 1921–1938.
Curtis, M.E., Cardott, B.J., Sondergeld, C.H., Rai, C.S., 2012. Development of organic porosity in the Woodford Shale with increasing thermal maturity. Int. J. Coal Geol. 103, 26–31.
Dai, J.X., Li, J., Luo, X., Zhang, W.Z., Hu, G.Y., Ma, C.H., Guo, J.M., Ge, S.G., 2005. Stable carbon isotope compositions and source rock geochemistry of the giant gas accumulations in the Ordos Basin, China. Org. Geochem. 36, 1617–1635.
Ding, W.L., Zhu, D.W., Cai, J.J., Gong, M.L., Chen, F.Y., 2013. Analysis of the developmental characteristics and major regulating factors of fractures in marine-continental transitional shale-gas reservoirs: a case study of the Carboniferous-Permian strata in the southeastern Ordos Basin, Central China. Mar. Pet. Geol. 45, 121–133.
Delvaux, D., Martin, H., Leplat, P., Paulet, J., 1990. Comparative Rock-Eval pyrolysis as an improved tool for sedimentary organic matter analysis. Org. Geochem. 16, 1221–1229.
Duan, Y., 2012. Geochemical characteristics of crude oil in fluvial deposits from Maling oilfield of Ordos Basin, China. Org. Geochem. 52, 35–43.
Duan, Y., Wang, C.Y., Zheng, C.Y., Wu, B.X., Zheng, G.D., 2008. Geochemical study of crude oils from the Xifeng oilfield of the Ordos Basin, China. J. Asian Earth Sci. 31, 341–356.
Gasparik, M., Bertier, P., Gensterblum, Y., Ghanizadeh, S., Krooss, B.M., Littke, R., 2014. Geological controls on the methane storage capacity in organic-rich shales. Int. J. Coal Geol. 123, 34–51.
Gasparik, M., Ghanizadeh, A., Bertier, P., Gensterblum, Y., Bouw, S., Krooss, B.M., 2012. High-pressure methane sorption isotherms of black shales from The Netherlands. Energy Fuels 26, 4995–5004.
Gong, Z.S., Zhu, W.L., Chen, P.P.H., 2010. Revitalization of a mature oil-bearing basin by a paradigm shift in the exploration concept. A case history of Bohai Bay, Offshore China. Mar. Pet. Geol. 27, 1011–1027.
Gregg, S.J., Sing, K.S.W., 1982. Adsorption Surface Area and Porosity. Academic Press, New York.
Guo, H.J., Wang, X.Z., Zhang, L.X., Jiang, C.F., Jia, W.L., Peng, P.A., Lei, Y.H., Luo, X.R., Cheng, M., 2014. Adsorption of N_2 and CO_2 on mature shales before and after extraction and its implication for investigations of pore structures. Geochimica 43, 408–414 (in Chinese with English abstract).
Hammes, U., Hamlin, H.S., Ewing, T.E., 2011. Geologic analysis of the Upper Jurassic Haynesville Shale in east Texas and west Louisiana. AAPG Bull. 95, 1643–1666.
Han, S.B., Zhang, J.C., Li, Y.X., Horsfield, B., Tang, X., Jiang, W.L., Chen, Q., 2013. Evaluation of Lower Cambrian shale in Northern Guizhou Province, South China: implications for shale gas potential. Energy Fuels 27, 2933–2941.
Jarvie, D.M., Hill, R.J., Ruble, T.E., Pollastro, R.M., 2007. Unconventional shale-gas systems: the Mississippian Barnett Shale of north-central Texas as one model for thermogenic shale-gas assessment. AAPG Bull. 91, 475–499.
Ji, L.M., Zhang, T.W., Milliken, K.L., Qu, J.L., Zhang, X.L., 2012. Experimental investigation of main controls to methane adsorption in clay-rich rocks. Appl. Geochem. 27, 2533–2545.
Kelemen, S.R., Walters, C.C., Ertas, D., Kwiatek, L.M., 2006a. Petroleum expulsion part 2. Organic matter type and maturity effects on kerogen swelling by solvents and thermodynamic parameters for kerogen from regular solution theory. Energy Fuels 20, 301–308.
Kelemen, S.R., Walters, C.C., Ertas, D., Freund, H., Curry, D.J., 2006b. Petroleum expulsion part 3. A model of chemically driven fractionation during expulsion of petroleum from kerogen. Energy Fuels 20, 309–319.
Lafargue, W., Espitalie, J., Broks, T., Nyland, B., 1994. Experimental simulation of primary migration. Org. Geochem. 22, 575–586.
Lafargue, E., Espitalie, J., Jacobsen, T., Eggen, S., 1990. Experimental simulation of hydrocarbon expulsion. Org. Geochem. 16, 121–131.
Lamberson, M.N., Bustin, R.M., 1993. Coalbed methane characteristics of Gates Formation coals, northeastern British Columbia: effect of maceral composition. AAPG Bull. 77, 2062–2076.

Li, D.S., 1996. Basic characteristics of oil and gas basins in China. J. Southeast Asian Earth Sci. 13, 299–304.
Liu, D., Yuan, P., Liu, H.M., Li, T., Tan, D.Y., Yuan, W.W., He, H.P., 2013. High-pressure adsorption of methane on montmorillonite, kaolinite and illite. Appl. Clay Sci. 85, 25–30.
Loucks, R.G., Reed, R.M., Ruppel, S.C., Jarvie, D.M., 2009. Morphology, genesis, and distribution of nanometer-scale pores in siliceous mudstones of the Mississippian Barnett shale. J. Sediment. Res. 79, 848–861.
Lu, X.C., Li, F.C., Watson, A.T., 1995. Adsorption measurements in Devonian Shales. Fuel 74, 599–603.
Mastalerz, M., He, L.L., Melnichenko, Y.B., Rupp, J.A., 2013. Porosity of coal and shale: insights from gas adsorption and SANS/USANS techniques. Energy Fuels 26, 5109–5120.
Montgomery, S.L., Jarvie, D.M., Bowker, K.A., Pollastro, R.M., 2005. Mississippian Barnett shale, Fort Worth Basin, north-central Texas: gas-shale play with multi-trillion cubic foot potential. AAPG Bull. 89, 155–175.
Pepper, A.S., Corvi, P.J., 1995. Simple kinetic-models of petroleum formation 3. Modeling an open system. Mar. Pet. Geol. 12, 417–452.
Prinz, D., Littke, R., 2005. Development of the micro- and ultramicroporous structure of coals with rank as deduced from the accessibility to water. Fuel 84, 1645–1652.
Prinz, D., Pyckhout-Hintzen, W., Littke, R., 2004. Development of the meso- and macroporous structure of coals with rank as analysed with small angle neutron scattering and adsorption experiments. Fuel 83, 547–556.
Rexer, T.F., Benham, M.J., Aplin, A.C., Thomas, K.M., 2013. Methane adsorption on shale under simulated geological temperature and pressure conditions. Energy Fuels 27, 3099–3109.
Rexer, T.F., Mathia, E.J., Aplin, A.C., Thomas, K.M., 2014. High-pressure methane adsorption and characterization of pores in Posidonia shales and isolated kerogens. Energy Fuels 28, 2886–2901.
Ritter, U., 2003. Solubility of petroleum compounds in kerogen: implications for petroleum expulsion. Org. Geochem. 34, 319–326.
Rodriguez, N.D., Philp, R.P., 2010. Geochemical characterization of gases from the Mississippian Barnett shale, Fort Worth Basin, Texas. AAPG Bull. 94, 1641–1656.
Ross, D.J.K., Bustin, R.M., 2007. Shale gas potential of the Lower Jurassic Gordondale Member, northeastern British Columbia, Canada. Bull. Can. Pet. Geol. 55, 51–75.
Ross, D.J.K., Bustin, R.M., 2008. Characterizing the shale gas resource potential of Devonian-Mississippian strata in the Western Canada sedimentary basin: application of an integrated formation evaluation. AAPG Bull. 92, 87–125.
Ross, D.J.K., Bustin, R.M., 2009. The importance of shale composition and pore structure upon gas storage potential of shale gas reservoirs. Mar. Pet. Geol. 26, 916–927.
Sandvik, E.I., Young, W.A., Curry, D.J., 1992. Expulsion from hydrocarbon sources – the role of organic absorption. Org. Geochem. 19, 77–87.
Selley, R.C., 2012. UK shale gas: the story so far. Mar. Pet. Geol. 31, 100–109.
Slatt, R.M., O'Brien, N.R., 2011. Pore types in the Barnett and Woodford gas shales: contribution to understanding gas storage and migration pathways in fine-grained rocks. AAPG Bull. 95, 2017–2030.
Strąpoć, D., Mastalerz, M., Schimmelmann, A., Drobniak, A., Hasenmueller, N.R., 2010. Geochemical constraints on the origin and volume of gas in the New Albany shale (Devonian-Mississippian), eastern Illinois Basin. AAPG Bull. 94, 1713–1740.
Tang, X., Zhang, B.S., Höök, M., Feng, L.Y., 2010. Forecast of oil reserves and production in Daqing oilfield of China. Energy 35, 3097–3102.
Thomas, M.M., Clouse, J.A., 1990. Primary migration by diffusion through kerogen: II. Hydrocarbon diffusivities in kerogen. Geochim. Cosmochim. Acta 54, 2781–2792.
Valenza, J.J., Drenzek, N., Marques, F., Pagels, M., Mastalerz, M., 2013. Geochemical controls on shale microstructure. Geology 41, 611–614.
Vishnyakov, A., Ravikovitch, P.I., Neimark, A.V., 1999. Molecular level models for CO_2 sorption in nanopores. Langmuir 15, 8736–8742.
Wang, H.D., Allen, J., Philp, R.P., 1995. An organic geochemical investigation of oils and source rocks from two Mesozoic formations of Shanganning Basin, China. J. Southeast Asian Earth Sci. 11, 277–288.
Wang, S.B., Song, Z.G., Cao, T.T., Song, X., 2013. The methane sorption capacity of Paleozoic shales from the Sichuan Basin, China. Mar. Pet. Geol. 44, 112–119.
Wang, X.Z., Zhang, J.C., Cao, J.Z., Zhang, L.X., Tang, X., Lin, L.M., Jiang, C.B., Yang, Y.T., 2012. A preliminary discussion on evaluation of continental shale gas resources: a case study of Chang 7 of Mesozoic Yanchang Formation in Zhiluo-Xiasiwan area of Yanchang. Earth Sci. Front. 19, 192–197 (in Chinese with English abstract).
Yao, S.P., Zhang, K., Hu, W.X., Fang, H.F., Jiao, K., 2009. Sedimentary organic facies of the Triassic Yanchang Formation in the Ordos Basin. Oil Gas Geol. 30, 74–84 (in Chinese with English abstract).
Yee, D., Seidle, J.P., Hanson, W.B., 1993. Gas sorption on coal and measurement of gas content. Hydrocarbons from coal. AAPG Stud. Geol. 38, 203–218.
Zhang, T.W., Ellis, G.S., Ruppel, S.C., Milliken, K., Yang, R.S., 2012. Effect of organic-matter type and thermal maturity on methane adsorption in shale-gas systems. Org. Geochem. 47, 120–131.
Zhang, W.Z., Yang, H., Fu, S.T., Zan, C.L., 2007. On the development mechanism of the lacustrine high-grade hydrocarbon source rocks of Chang 9 member in Ordos Basin. Sci. China Ser. D Earth Sci. 50, 39–46.
Zhang, W.Z., Yang, H., Hou, L.H., Liu, F., 2009. Distribution and geological significance of 17α(H)-diahopanes from different hydrocarbon source rocks of Yanchang Formation in Ordos Basin. Sci. China Ser. D Earth Sci. 52, 965–974.
Zou, C.N., Yang, Z., Cui, J.W., Zhu, R.K., Hou, L.H., Tao, S.Z., Yuan, X.J., Wu, S.T., Lin, S.H., Wang, L., Bai, B., Yao, J.L., 2013. Formation mechanism, geological characteristics and development strategy of nonmarine shale oil in China. Pet. Explor. Dev. 40, 15–27.